

# Dynamic constitutive behavior of Ti/TiB FGM under thermo-mechanical loading

Addis Kidane · Arun Shukla

Received: 18 December 2007 / Accepted: 31 January 2008 / Published online: 28 February 2008  
© Springer Science+Business Media, LLC 2008

**Abstract** An experimental investigation is conducted to evaluate the thermo-mechanical constitutive behavior of a functionally graded material (FGM) under dynamic loading. Cylindrical specimens are machined from a titanium/titanium mono-boride (Ti/TiB)-layered FGM plate using electrical discharge machining (EDM). A Split Hopkinson Pressure Bar (SHPB) apparatus with infrared (IR) spot heaters is used to investigate the effect of temperature on mechanical response of the FGM material. A series of experiments are conducted at different temperatures and the stress–strain relation for different temperatures is obtained. The material showed high thermal softening at elevated temperatures resulting in a large reduction in compressive strength and an increase in failure strain.

## Introduction

Functionally graded materials (FGMs) are materials, which have continuously or discretely varying mechanical and thermal properties in a specific direction. Ideally, by grading the composition from one surface to another, it is possible to create a material suitable for a particular application. This type of material was first proposed in Japan in 1987 for space access vehicles that can operate reliably in combined thermal and mechanical loadings. Typically, FGMs are made of a metal and a ceramic as opposite faces with the intermediate zones consisting

of varying volume fractions of constituents. Titanium/titanium mono-boride (Ti/TiB) is one of the FGMs which is currently in use. This material has desirable properties of ceramic, such as hardness, corrosion resistance, and high melting temperature, without losing the required properties of metallic titanium, such as good fracture toughness, machinability, and weldability.

For efficient design of structures using FGM materials a fundamental understanding of the properties of FGM materials at different loading conditions is required. To date research on FGM materials has focused mostly on quasi-static problems with very few studies in the dynamic regime. Also, most of the mechanics studies relate to crack problems. Delale and Erdogan [1], Eischen [2], and Jin and Noda [3] solved crack problems for nonhomogeneous materials under quasi-static mechanical loading. All these investigations concluded that the inverse-square root singularity at the crack is not affected by nonhomogeneity. For propagating cracks in FGMs, Parameswaran and Shukla [4] and Chalivendra et al. [5] developed the structure of the first stress invariant and the out-of-plane displacement. In their study they brought out the effects of nonhomogeneity through an asymptotic analysis. Lee [6] developed nonhomogeneity-specific terms for individual stress and displacement components using displacement potentials. Recently, Shukla and Jain [7] and Chalivendra and Shukla [8] has developed transient field equations for cracks propagating at arbitrary velocities. Chalivendra [9] developed an asymptotic analysis of the transient out-of-plane displacement fields for a curved crack propagating at arbitrary velocity in FGMs. A review paper by Shukla et al. [10] presents a comprehensive summary of dynamic fracture studies in FGMs.

There are few studies related to the stress and displacement fields due to applied loads in graded materials.

---

A. Kidane · A. Shukla (✉)  
Dynamic Photomechanics Laboratory, Department  
of Mechanical Engineering and Applied Mechanics,  
The University of Rhode Island, Kingston, RI 02881, USA  
e-mail: shuklaa@egr.uri.edu

For instance Wang et al. [11] present the solution for displacements and stresses in an FGM subjected to a vertical point load in a continuously inhomogeneous transversely isotropic half-space with Young's and shear moduli varying exponentially with depth. Horgan and Chan [12] investigate the effects of material inhomogeneity on the response of linearly elastic isotropic hollow circular cylinders under uniform internal or external pressure. Li et al. [13] examined the mechanical behavior of layered plates made of metal-ceramic composites with the volume fraction of ceramic reinforcement varying through thickness direction under impulse loading. Chi and Chung [14] study the mechanical behavior of functionally graded material plate under transverse loading.

There are very few studies on the properties of FGM under thermal or thermo-mechanical loading. Jain et al. [15] developed the stress field equations for quasi-static cracks under thermo-mechanical loading in FGMs. Praveen and Reddy [16] carried out the nonlinear transient analysis of stress and deflection for a functionally graded ceramic-metal plate under thermal loading using the finite element method (FEM). They found that the response of the plates with material properties between those of the ceramic and metal is not intermediate to the response of the ceramic and metal plates. Dai et al. [17] also presented thermo-mechanical analysis of deflections under different loadings in FGM plates containing distributed piezoelectric sensors and actuators using element-free Galerkin method.

In this paper an experimental investigation on the dynamic constitutive behavior of Ti/TiB FGM under thermo-mechanical loading is presented. SHPB apparatus with infrared spot heating system is used to investigate the constitutive properties of the FGM at different temperatures. The material exhibited thermal softening at higher temperatures, which results in a decrease in flow stress and an increase in failure strain. The effect of machining conditions on the constitutive behavior is also demonstrated in these experiments.

### Material and specimen geometry

The layered (Ti/TiB) functionally graded material used in this study is supplied by BAE Systems in the form of 3.175-mm-thick plates. Hill et al. [18] have explained the fabrication technique for this material and their procedure is presented below. Tape cast layer composed of varying mixtures of titanium and titanium diboride powders are placed on top of a commercially pure titanium metal plate. The assembled laminate is hot pressed at 1,578 K at a pressure of 13.8 MPa. To facilitate densification at this temperature, a proprietary sintering aid containing nickel is added to the starting powders. This material creates a liquid

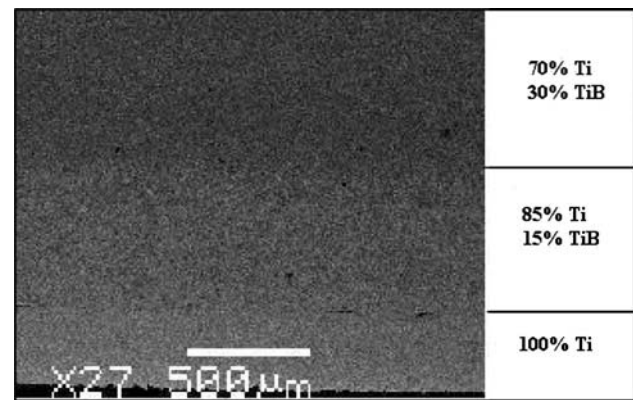


**Fig. 1** Scanning electron microscope image of layer 1 (TiB 0%), layer 2 (TiB 15%), and layer 3 (TiB 30%)

**Table 1** Composition and elastic properties of Ti/TiB FGM

| Layer no. | Vol.%Ti | Vol.% TiB | Thickness (mm) | <i>E</i> (GPa) | <i>v</i> |
|-----------|---------|-----------|----------------|----------------|----------|
| 1         | 100     | 0         | 0.2032         | 106            | 0.340    |
| 2         | 85      | 15        | 0.3810         | 170            | 0.278    |
| 3         | 70      | 30        | 0.3810         | 227            | 0.238    |
| 4         | 55      | 45        | 0.3810         | 262            | –        |
| 5         | 40      | 60        | 0.3810         | 289            | –        |
| 6         | 25      | 75        | 0.3810         | 303            | 0.152    |
| 7         | 15      | 85        | 1.0668         | 316            | 0.140    |

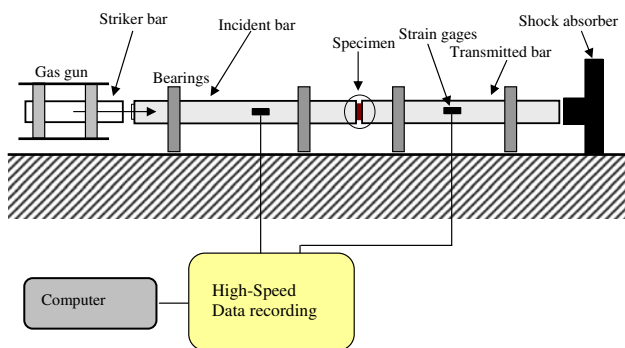
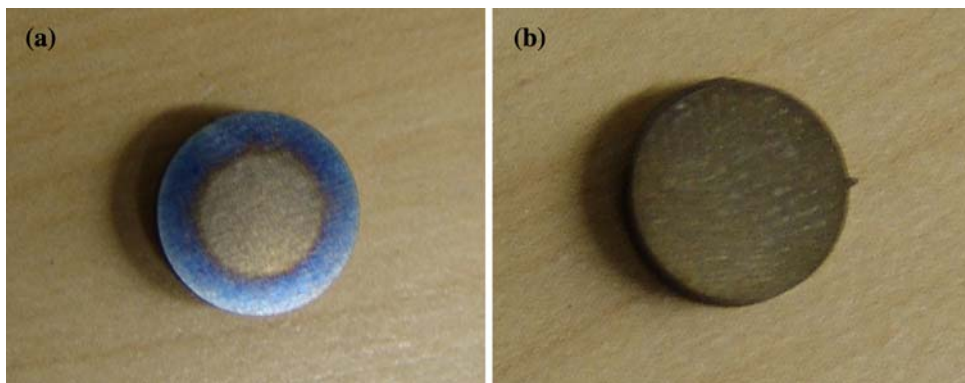
phase at 1,215 K that also catalyzes the reaction of titanium and TiB<sub>2</sub> to form TiB with virtually no residual TiB<sub>2</sub>. The resulting FGM is composed of seven layers ranging from pure Ti on one side to 85% TiB on the other [18]. The material used in our studies shows no clear or distinct interface between the layers as shown in Fig. 1. Table 1 shows the composition and the physical properties of each layer of the FGM as provided by the vendor and [18].

Cylindrical specimens with diameter of 7.62 mm and thickness of 3.175 mm are machined from the FGM plate discussed above. An electrical discharge machining (EDM) technique is used to machine the specimens. The thickness of the specimen is selected from the available FGM plate thickness, where the diameter of the specimen is selected based on the SHPB theory to assure uniform loading and constant strain rate. The first batch of specimens is machined using wire EDM and cooled by flooding (Fig. 2a). The second batch of specimens is machined with wire EDM with the material fully immersed in a coolant (Fig. 2b).

### Experimental procedure

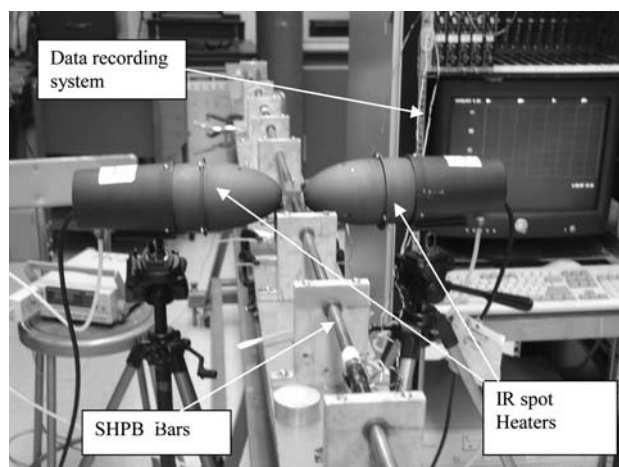
SHPB apparatus with infrared spot heaters is used to investigate the dynamic behavior of Ti/TiB FGM at room

**Fig. 2** Wire EDM-machined specimens (a) cooled by flooding, (b) cooled by fully immersing in coolant



**Fig. 3** Schematic of Split Hopkinson Pressure Bar

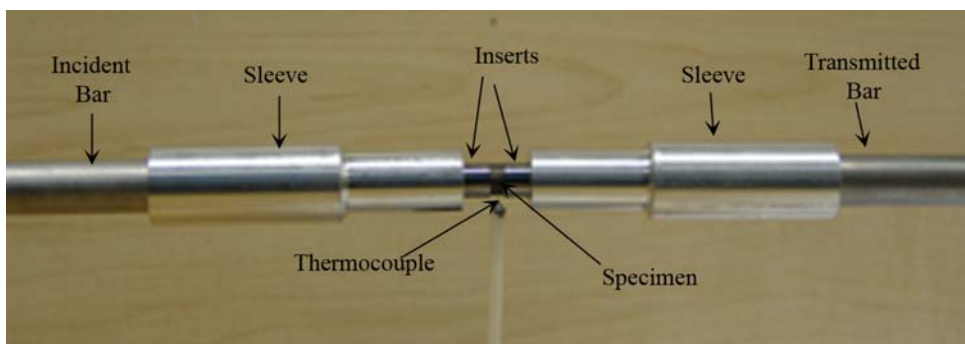
and at elevated temperatures. In the present study, the technique used by Lennon and Ramesh [19] and Mostafa et al. [20] is adapted. The schematic description of the SHPB in our lab is shown in Fig. 3 and the set-up with infrared (IR) spot heaters is shown in Fig. 4. The IR spot heaters have a circular cut shields that can concentrate a heat flux as high as 650 watts per 6.45 square centimeters at the focal point with a 6.35-mm diameter. The bars are made up of 12.7-mm diameter marringing steel having nominal yield strength of 2,500 MPa. The striker bar is 101.6-mm long, while the incident and transmitter bars are 1.27-m long. The striker bar is propelled using an air-operated gun. Two strain gages are placed on both the incident and the transmitter bars at equal distance from the bar-specimen assembly. These gages are placed at 180° to each other to avoid the bending effect on the strain data. The strain signals are recorded using a Vishay



**Fig. 4** Split Hopkinson Pressure Bar with heater assembly

2301A signal-conditioning amplifier that connects with an oscilloscope. The specimen is sandwiched between the two bars. However, during the elevated temperature testing two carbide inserts are placed between the two bars and the specimen is sandwiched between the inserts. The inserts are used to eliminate the temperature gradient in the bars. The inserts are impedance matched to the bars and hence do not disturb the incident, transmitted, and reflected wave profiles. The insert and the bar are placed in a sleeve to assist in alignment. The assembly of the carbide inserts with the specimen and the position of the thermocouple is shown in Fig. 5.

**Fig. 5** Specimen-carbide inserts, thermocouple, and sleeve assembly



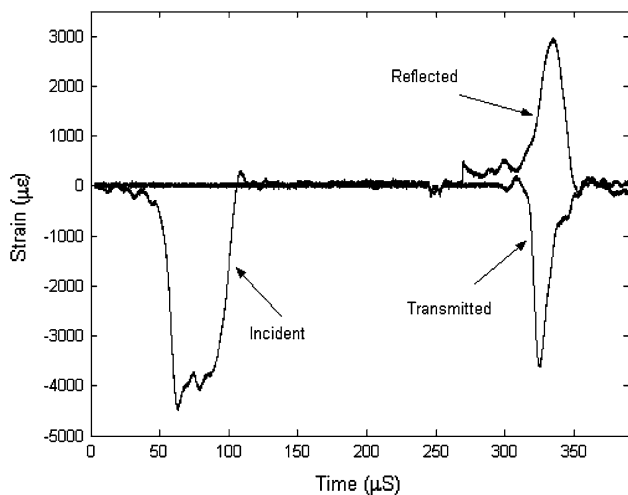


**Fig. 6** Typical strain pulse profiles obtained during an experiment

For the elevated temperature experiment, the specimen is heated up to the desired temperature (usually about 30–40 °C higher than the test temperature) and the bars are brought manually in contact with the inserts-specimen-inserts assembly. The temperature of the specimen is monitored by a 0.127 mm chromel–alumel thermocouple, which is attached to the specimen using high-temperature epoxy. Digital camera is used to record the temperature reading and to monitor the sequence of loading of the specimen. The exact temperature on the specimen at which the load applied is found from the record. Boron nitride is used as the lubrication between specimen–inserts and inserts–bar assembly for all elevated temperature experiments. In most of the experiments it takes less than two minutes to heat the specimen to the required temperature. It takes less than 10 s to bring the bars in contact with the specimen and fire the gun.

Using the above configuration a series of experiments were conducted. For all experiments a clay-pulse shaper is placed on the impact face of the incident bar. The pulse shaper smoothes the relative sharp front of the incident stress wave, thus allowing high strain-rate experiments to be conducted at near constant strain rates [20]. This also helps the premature failure of the relatively brittle Ti/TiB FGM, especially during the early part of stress wave loading [20]. A typical strain record from one of the experiments is shown in Fig. 6.

## Results and discussion

A series of eight experiments are conducted at four different temperatures on specimens machined by wire EDM and cooled by flooding. The stress–strain curves obtained

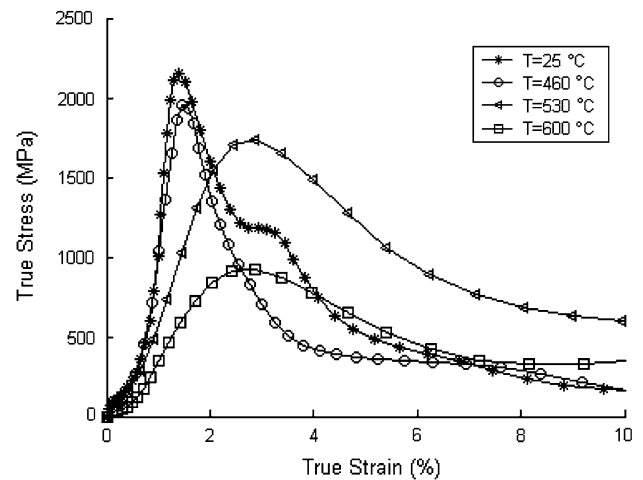


**Fig. 7** True stress–True strain curve as a function of temperature (specimen cooled by flooding during EDM)

from the dynamic experiments with strain rate of about  $3 \times 10^3$  per sec are shown in Fig. 7. The stress–strain curves show a monotonic increase till failure is reached. In all these experiments failure was achieved. The unloading part of the curves after failure is not meaningful. At room temperature a failure stress of 2,150 MPa and a failure strain of 1.4% is observed. As the temperature increases a reduction in the failure stress and an increase in the failure strain is observed. For example at 600 °C a failure stress of 910 MPa and a failure strain of 2.6% are observed. In all the room temperature experiments the specimens fail completely leaving small fragments as shown in Fig. 8. It was also observed that the fragmentation process even at room temperature was associated with a flash of light. A typical flash of light during failure was recorded using a



**Fig. 8** A typical failed specimen at room temperature under dynamic loading

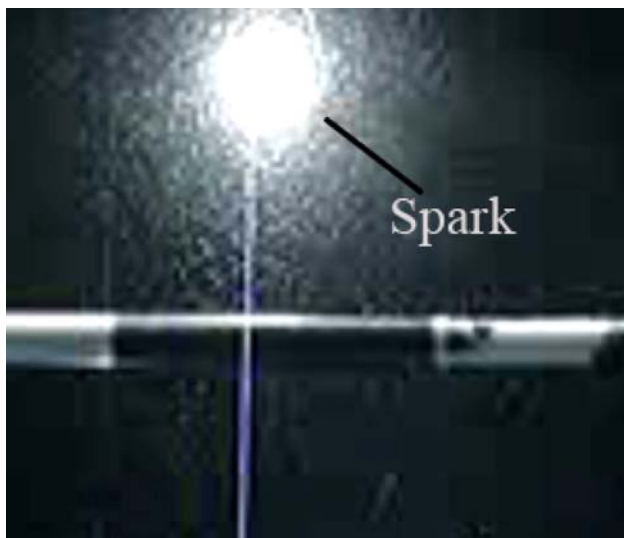


**Fig. 9** A flash of light produced during room temperature dynamic experiment of a specimen machined by EDM and cooled by flooding

digital camera and is shown in Fig. 9. The occurrence of flash led us to believe that high residual stresses were present in the material, and these could have been created during the machining process. The material fabrication technique is believed to create a relatively stress-free material. The coloration on the edge of the specimen shown in Fig. 2a indicates a heat-affected zone generated during machining by wire EDM.

To investigate the effect of machining technique on the behavior of the material another batch of samples was machined using EDM with the material fully immersed in the coolant. A series of eight experiments were again conducted using these specimens at four different temperatures. Figure 10 shows the dynamic compressive stress–strain curve of the materials at different temperatures. At room

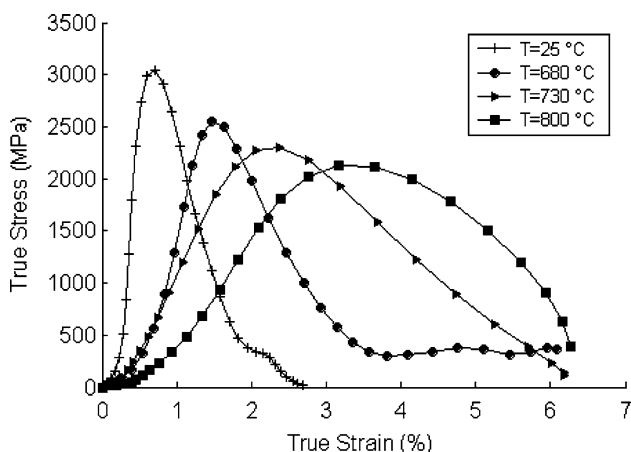


**Fig. 10** True stress–True strain curve as a function of temperature (specimen fully immersed in coolant during EDM)

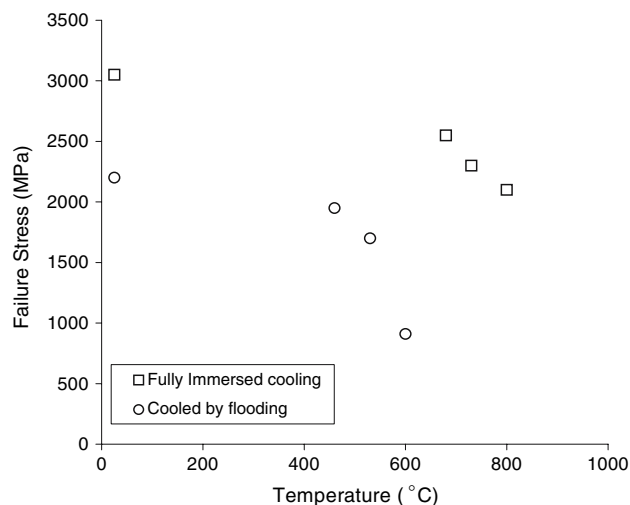


**Fig. 11** Failure stress as a function of temperature

temperature a failure stress of 3,050 MPa and a failure strain of 1.2% are obtained. As the temperature increases, the ductility of the material increases and results in an increase in the failure strain and a decrease in failure stress. For example, at the testing temperature of 730 °C a failure stress of 2,300 MPa and a failure strain of 2.6% are observed, and at 800 °C a failure stress of 2,100 MPa and a failure strain of 3.4% are obtained. There was no flash of light observed during testing of these specimens.

Figure 11 shows the effect of temperature on the failure stress of Ti/TiB for both the machining cases considered. Both the curves show a similar trend that the failure stress decreases as the temperature increase. In the case of specimen machined by EDM and cooled by flooding the failure stress at 600 °C is reduced by 54% compared with the room temperature failure stress. For fully immersed cooling EDM specimen the failure stress at 800 °C is reduced by 30% compared with the room temperature failure stress.

### Post-failure analysis

Photographs of the fracture specimen were taken for post-failure analysis. In all the room temperature experiments the specimens fractured completely, leaving small fragments as shown in Fig. 8. However in the case of high-temperature experiments the specimens fracture leaving the fragments loosely bonded as shown in Fig. 12. This indicates at higher temperatures the material is thermally softened and shows a ductile failure. Figure 13 shows a micrograph of a fragment from a room temperature experiment. From the figure it is observed that the cracks run predominantly in the loading direction, which is perpendicular to the interface of layers, indicating the bonding of the interface is strong.

Scanning Electron Microscopic (SEM) images were taken of the fractured specimens tested at four different temperatures. Figure 14 shows SEM images of four high-temperature specimens taken at a magnification of 1,000.



**Fig. 12** Typical failed specimen during dynamic loading at elevated temperatures

The post mortem examination of the failed specimens showed that at room temperature and at 460 °C the specimens fracture by cleavage (Fig. 14a and b). The fracture surfaces from specimens tested at temperatures of 730 and 800 °C are shown in Fig. 14c and d, respectively, and both of them indicate a ductile failure mode. A number of large smooth surfaces observed in Fig. 14c and d are believed to have been caused by plastic shear [21]. These smooth surfaces are shown at higher magnification (5,000 times) in Fig. 15a and b.

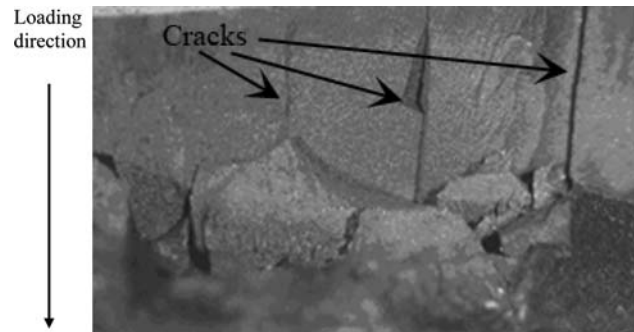


**Fig. 13** Typical fracture surface of Ti/TiB specimen

**Fig. 14** SEM images, at a magnification of 1,000, of fracture surface of four different specimens tested at four different temperatures

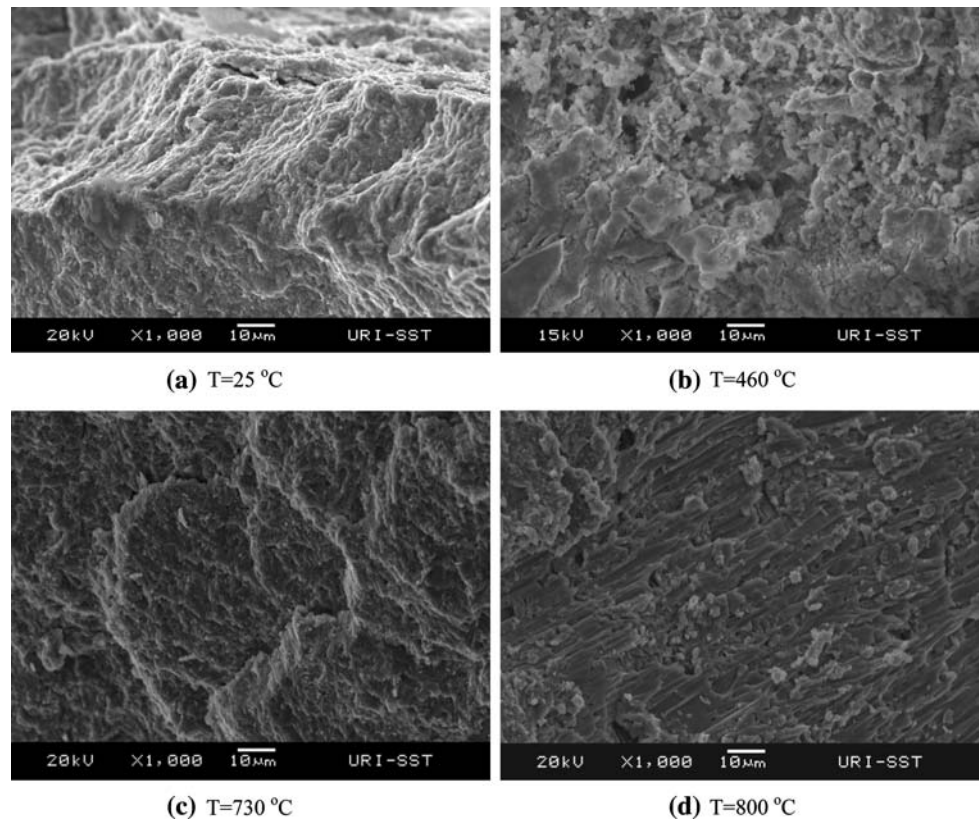
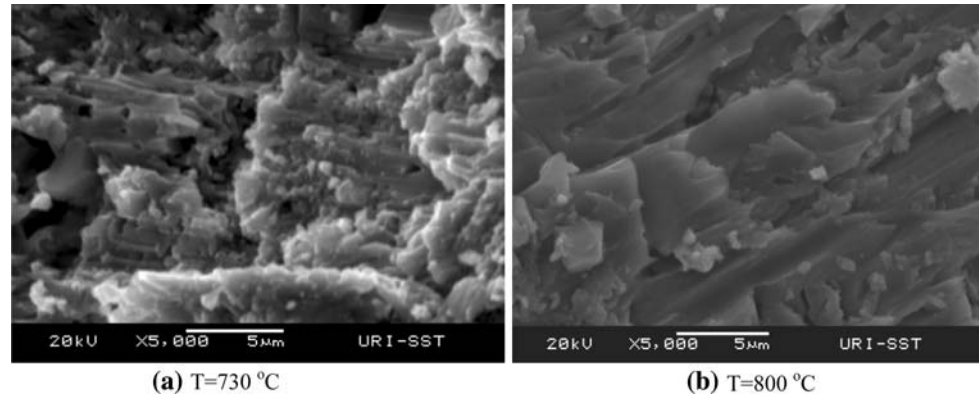


**Fig. 15** SEM images, at a magnification of 5,000, of fracture surface of specimens tested at two different temperatures



## Conclusions

The dynamic constitutive behavior of Ti/TiB FGM under thermo-mechanical loading is investigated. SHPB apparatus along with spot heaters is utilized to study the dynamic constitutive behavior of the material in the temperature range from 25 °C to 800 °C. The findings are summarized and presented as follows:

1. There are no distinct interfaces between the layers of the FGM material investigated. The bonds between the layers are strong and the cracks run predominantly perpendicular to the layers during fracture.
2. Samples cut by wire EDM and cooled by flooding and tested at 25 °C show a failure stress of 2,150 MPa and a failure strain of 1.4%. At 600 °C the same sample type shows a failure stress of 910 MPa and a failure strain of 2.6%. This represents a 54% reduction in failure stress and an 85% increase in failure strain.
3. Fully immersed cooled EDM specimens tested at 25 °C show a failure stress of 3,050 MPa and a failure strain of 1.25%. At 800 °C a failure stress of 2,100 MPa and a failure strain of 3.4% are observed. This represents a 30% reduction in failure stress and a 125% increase in failure strain.
4. The FGM material showed thermal softening at higher temperature with a decrease in failure stress and an increase in failure strain for both the machining cases considered.
5. The specimens machined from fully immersed cooling EDM show superior compressive strength at room and at elevated temperatures when compared to the sample machined by EDM with flooding. This is due to the presence of residual stresses in the specimens that were not fully immersed for cooling during machining.

6. The post mortem SEM images indicate cleavage-type failure in specimens tested at 460 °C and below. The failure mechanism changes to ductile at higher temperatures.

**Acknowledgement** The financial support of the Air Force Office of Scientific Research under grant # FA9550-06-1-0162 is gratefully acknowledged.

## References

1. Delale F, Erdogan F (1983) *J Appl Mech* 50:67
2. Eischen JW (1987) *Int J Frac* 34(3):3
3. Jin ZH, Noda N (1994) *J Appl Mech (Trans ASME)* 61:738
4. Parameswaran V, Shukla A (1999) *Mech Mater* 31:579
5. Chalivendra VB, Shukla A, Parameswaran V (2002) *J Elasticity* 69:99
6. Lee KH (2004) *Int J Solids Struct* 41:2879
7. Shukla A, Jain N (2004) *Int J Impact Eng* 30:777
8. Chalivendra VB, Shukla A (2005) *J Appl Mech* 72:237
9. Chalivendra VB (2007) *Int J Solids Struct* 44:465
10. Shukla A, Jain N, Chona R (2007) *Strain* 43:76
11. Wang CD, Tzeng CS, Pan E, Liao JJ (2003) *Int J Rock Mech Min Sci* 40:667
12. Horgan CO, Chan AM (1999) *J Elasticity* 55:43
13. Li Y, Ramesh KT, Chin ESC (2001) *Int J Solids Struct* 38:6041
14. Chi SH, Chung YL (2006) *Int J Solids Struct* 43:3657
15. Jain N, Chona R, Shukla A (2006) *J ASTM Int* 03
16. Praveen G, Reddy J (1998) *Int J Solids Struct* 35:4457
17. Dai KY, Liu GR, Han X, Lim KM (2005) *Comp and Struct* 83:1487
18. Hill M, Carprntr R, Pailino G, Munir Z, Gibeling J (2002) Fracture resistance testing of monolithic and composite brittle materials. ASTM STP 1409
19. Lennon AM, Ramesh KT (1998) *Int J Plasticity* 14:1279
20. Shazly M, Prakash V, Draper S (2004) *Int J Solids Struct* 41:6485
21. *Metals Handbook, Fractography and Atlas of Fractographs*, ASM Vol. 9, 8th edn (1974)